The Astrophysical Journal, 699:298–304, 2009 July 1 doi:10.1088/0004-637X/699/1/298

A COMPARISON OF THE INITIAL SPEED OF CORONAL MASS EJECTIONS WITH THE MAGNETIC FLUX AND MAGNETIC HELICITY OF MAGNETIC CLOUDS

S.-K. Sung[1,2,3], K. Marubashi[1], K.-S. Cho[1], Y.-H. Kim[1], K.-H. Kim[1,3], J. Chae[2], Y.-J. Moon[3], and I.-H. Kim[3]
[1] Korea Astronomy & Space Science Institute, Space Science Division, Solar & Space Weather Research Group, Daejeon, Korea
[2] Astronomy Program, Department of Physics and Astronomy, Seoul National University, Seoul, Korea
[3] School of Space Research, Kyung Hee University, Yongin, Gyeonggi 446-701, Korea, sksung@khu.ac.kr
Received 2008 May 19; accepted 2009 April 13; published 2009 June 11

ABSTRACT

To investigate the relationship between the speed of a coronal mass ejection (CME) and the magnetic energy released during its eruption, we have compared the initial speed of CMEs (V_{CME}) and the two parameters of their associated magnetic clouds (MC), magnetic flux (F_{MC}), and magnetic helicity per unit length ($|H_{MC}|/L$), for 34 pairs of CMEs and MCs. The values of these parameters in each MC have been determined by fitting the magnetic data of the MC to the linear force-free cylindrical model. As a result, we found that there are positive correlations between V_{CME}^2 and F_{MC}, and between V_{CME}^2 and $|H_{MC}|/L$. It is also found that the kinetic energy of CMEs (E_{CME}) is correlated with F_{MC} and $|H_{MC}|/L$ of the associated MC. In contrast, we found no significant correlation between $\langle V_{MC}\rangle^2$ and F_{MC}, nor between $\langle V_{MC}\rangle^2$ and $|H_{MC}|/L$. Our results support the notion that the eruption of a CME is related to the magnetic helicity of the source active region.

Key words: Sun: coronal mass ejections – Sun: magnetic fields – solar–terrestrial relations

1. INTRODUCTION

The Sun expels mass, magnetic flux, and magnetic helicity to interplanetary space through coronal mass ejections (CMEs). When CMEs are observed by satellites at 1 AU, they are called interplanetary coronal mass ejections (ICMEs) or, more frequently, magnetic clouds (MCs). CMEs are one of the most interesting phenomena of the solar activity because they cause many kinds of space weather disturbances.

It is generally accepted that CMEs are produced by a loss of stability or equilibrium of the coronal magnetic field. The speed of a CME reflects the work done to it during the eruption. The work must have come from the free magnetic energy. Venkatakrishnan & Ravindra (2003) found that there is a positive correlation between the potential field magnetic energy of the active region (AR) and the CME speed, but a more recent study (Liu 2007) showed that there is no such correlation. Liu (2007) noted that there is a correlation between free energy densities of ARs and the CME speeds for eight events the free energy density of which is available. Using numerical simulations, Phillips et al. (2005) showed that the magnetic free energy is responsible for initiating CMEs. For the filament-associated CMEs, the speeds are strongly correlated with the average magnetic field strength in the filament channel (Chen 2006). Recently, by investigating 18 two-ribbon flares associated with CMEs, Su et al. (2007) showed that the intensity of flare/CME events may depend on the released free magnetic energy. Basically all of these studies support the idea that the free magnetic energy controls the solar eruption phenomena.

We note that the free magnetic energy is determined by the scale of the magnetic system as well as the degree of deviation of the field from the potential configuration (nonpotentiality). The scale of the magnetic system may be quantified by its magnetic flux, and the nonpotentiality may be coarsely quantified by the magnetic helicity of the system.

It is useful that magnetic helicity as well as magnetic flux is fairly well conserved (Berger 1984). Mandrini et al. (2005) compared the helicity loss in the solar corona due to a CME with magnetic helicity of a MC at 1 AU and reported that they were in good agreement. Luoni et al. (2005) traced magnetic helicity from the solar corona to interplanetary space for two cases, and found that the magnetic helicities in the corona and in interplanetary space agree within a factor of 2 (4.5×10^{42} Mx^2 in the corona and 8.5×10^{42} Mx^2 for the MC with same sign).

It is very likely that a MC is magnetically connected to its source region in the solar corona. A number of theoretical studies of CMEs have suggested that MCs are magnetic flux ropes extending from the solar corona (Chen 1989, 1996; Forbes & Priest 1995; Forbes 2000; Lin et al. 2004; Lynch et al. 2004). Lindsay et al. (1999) reported a possible relationship between the speed of CMEs and the magnitude of the interplanetary magnetic field (IMF) in the associated ICMEs. Yurchyshyn et al. (2004) compared B_z component of IMF near the front edge of an interplanetary ejecta and the projected speeds for 14 halo CMEs, and found a good correlation between them.

In the present paper, we investigate the relationship between the initial speed of CMEs and the magnetic flux and magnetic helicity of their associated MCs. We select 34 CME–MC pairs and fit the magnetic data of every MC to a cylindrical flux rope model to obtain the parameters of the MC.

2. DATA AND ANALYSIS

In this study, we have analyzed 34 pairs of CMEs and MCs observed during the period from 1997 to 2005. These events were selected from the archival data either published in the previous studies (Cane & Richardson 2003; Manoharan et al. 2004; Kim et al. 2007; Qiu et al. 2007; Zhang et al. 2007) and the MC list of *WIND* MFI Team.[4] To avoid probable errors due to the ambiguity in the identification of CME–MC pair, we have selected only those events for which the same CME–MC pair is identified in at least two references. For the fitting of MCs we used 1 hr averaged data of solar wind plasma and magnetic field taken either by the Solar Wind Experiment (SWE; Ogilvie et al. 1995) and the Magnetic Field Investigation (MFI; Lepping

[4] http://lepmfi.gsfc.nasa.gov/mfi/mag_cloud_pub1.html

Table 1
CME and MC Event Information

Event No.	CME Year	CME Apperance Time[b]	CME V_{CME} (km s^{-1})	CME E_{CME} (erg)	CME AR Sigmoid	MC Start Time	MC End Time	MC Duration (hr)	MC $\langle V_{MC} \rangle$ (km s^{-1})	SC[a]
1	1997	Jan 6 15:10	136	5.4E+28	S	Jan 10 5hr	Jan 11 2hr	21	440.3	W
2	1997	May 12 5:30	464	4.5E+30	Inv-S	May 15 9hr	May 16 1hr	16	463.6	W
3	1997	Jul 30 4:45	104	4.5E+28	Inv-S	Aug 3 14hr	Aug 4 2hr	12	434.1	W
4	1997	Sep 17 20:28	377	1.9E+30	S	Sep 21 22hr	Sep 23 2hr	28	415.5	W
5	1997	Sep 28 1:08	359	2.6E+30	Inv-S	Oct 1 17hr	Oct 2 23hr	30	449.9	W
6	1997	Oct 6 15:28	293	1.2E+30	S	Oct 10 22hr	Oct 12 0hr	26	399.9	W
7	1997	Nov 4 6:10	785	2.3E+31	S	Nov 7 5hr	Nov 8 11hr	30	425.8	W
8	1997	Nov 19 12:27	150	9.1E+28	S	Nov 22 18hr	Nov 23 12hr	18	506.4	W
9	1998	Jan 2 23:28	438	5.3E+30	...	Jan 7 3hr	Jan 8 12hr	29	377.2	W
10	1998	Feb 12 15:55	82	...	S	Feb 17 10hr	Fev 18 13hr	27	394.9	A
11	1998	Feb 28 12:48	176	7.7E+28	...	Mar 4 19hr	Mar 6 5hr	34	335.8	A
12	1998	Apr 29 16:58	1374	9.8E+31	Inv-S	May 2 12hr	May 3 21hr	33	511.0	A
13	1998	Jun 21 5:35	192	4.1E+29	Inv-S	Jun 24 13hr	Jun 25 22hr	33	464.8	A
14	1998	Oct 15 10:04	262	...	Inv-S	Oct 19 4hr	Oct 19 13hr	9	405.8	A
15	1998	Nov 5 20:44	1118	...	S	Nov 8 18hr	Nov 10 1hr	31	461.6	A
16	1998	Nov 9 18:18	325	...	S	Nov 13 4hr	Nov 14 6hr	26	380.4	A
17	1999	Apr 13 3:30	291	...	Inv-S	Apr 16 22hr	Apr 17 18hr	20	409.3	A
18	2000	Feb 17 20:06	728	...	S	Feb 21 16hr	Feb 22 14hr	22	374.9	W
19	2000	Jul 14 10:54	1674	1.9E+32	Inv-S	Jul 15 19hr	Jul 16 12hr	17	850.9	A
20	2000	Jul 25 3:30	528	2.3E+30	Inv-S	Jul 28 15hr	Jul 29 7hr	16	460.6	A
21	2000	Aug 9 16:30	702	1.7E+31	Inv-S	Aug 12 5hr	Aug 13 12hr	31	576.8	A
22	2000	Sep 29 21:50	173	1.0E+29	...	Oct 3 17hr	Oct 05 5hr	36	403.6	W
23	2000	Oct 9 23:50	798	4.6E+31	S	Oct 13 16hr	Oct 14 16hr	24	401.9	A
24	2000	Oct 25 8:26	770	5.1E+31	Inv-S	Oct 29 0hr	Oct 29 22hr	22	383.9	W
25	2000	Nov 3 18:26	291	2.1E+30	Inv-S	Nov 6 22hr	Nov 7 18hr	20	527.7	A
26	2001	Mar 16 3:50	271	3.9E+29	...	Mar 19 19hr	Mar 22 6hr	59	357.9	A
27	2001	Apr 19 12:30	392	2.1E+30	...	Apr 22 0hr	Apr 23 00hr	24	357.5	A
28	2001	Apr 26 12:30	1006	3.5E+31	S	Apr 29 0hr	Apr 29 14hr	14	622.5	A
29	2002	Mar 15 23:06	957	...	...	Mar 19 5hr	Mar 20 15hr	34	380.5	A
30	2002	Mar 20 17:54	603	...	...	Mar 24 3hr	Mar 25 22hr	43	434.7	A
31	2002	Apr 15 3:50	720	5.0E+30	...	Apr 18 1hr	Apr 19 11hr	34	470.3	A
32	2003	Nov 18 8:50	1660	3.3E+32	S	Nov 20 11hr	Nov 21 1hr	14	577.2	A
33	2004	Nov 7 16:54	1759	2.2E+32	...	Nov 9 20hr	Nov 10 9hr	13	762.9	A
34	2005	May 13 17:12	1689	...	Inv-S	May 15 6hr	May 16 12hr	30	777.0	A
Average			637	4.15E+31				25.9	470.5	

Notes.
[a] A and W represent *ACE* and *WIND* satellites, respectively.
[b] Format is month day hour:minute.

et al. 1995) on the *WIND* spacecraft, or by the Solar Wind Electron Proton Alpha Monitor (SWEPAM; McComas et al. 1998) and the Magnetic Field Experiment (MAG; Smith et al. 1998) on the *Advanced Composition Explorer* (*ACE)* spacecraft. The initial speed and kinetic energy of each CME were taken from the CME catalog of the *Solar and Heliospheric Observatory* (*SOHO*) Large Angle and Spectrometric Coronagraph Experiment (LASCO).[5]

Table 1 presents the list of the CME–MC pairs. The first six columns show event identification number, year, CME appearance time, CME initial speed, CME kinetic energy, and AR sigmoid type. V_{CME} is the linear speed of CME in the catalog. V_{CME} varied from 82 to 1759 km s^{-1} with average speed of 637 km s^{-1}, and E_{CME} from 4.5×10^{28} to 3.3×10^{32} erg with the average of 4.2×10^{31} erg. To identify the handedness of the presumed magnetic flux rope in an AR, we use the coronal flux rope (CFR) model (Titov & Dèmoulin 1999). According to Pevtsov & Canfield (2001) and Kang et al. (2006), the magnetic chirality of MC is consistent with that of the AR by adopting the CFR model. In the CFR model, the projected magnetic flux rope has a sigmoidal shape, that is, an *S* shape when the flux rope is right-handed and an inverse-*S* shape when left-handed. We used the X-ray images of *Yohkoh* Soft X-ray Telescope (SXT) and *GOES* Solar X-ray Imager (SXI) and identified 25 sigmoids. For the other nine events, either X-ray images were not available (Events 9, 29, 30, 31) or sigmoidal structures were not discernable (Events 11, 22, 26, 27, 33). We found that 13 of 25 sigmoids are of inverse-*S* shape. Figure 1 shows an example of an inverse-*S* shape sigmoid (left-handed flux rope) that is related to the CME occurred on 2000 July 14.

The next five columns indicate the start and end times of the CME, the duration and mean velocity of the MC ($\langle V_{MC} \rangle$), and the name of the spacecraft providing the data, respectively. Although we use the same MCs from published list, we adopt the start and end times that may be a little different from the previous studies. This is because we use a different MC fitting method and we found that the adjustment of the time span is necessary sometimes for the best fitting result. The duration of the time span for each MC (t_d) ranges from 9 to 59 hr with a

[5] http://cdaw.gsfc.nasa.gov/CME_list/

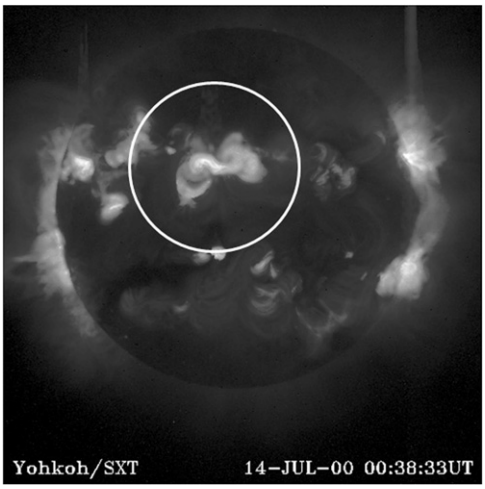

Figure 1. *Yohkoh*/SXT image at 00:38:33 UT on 2000 July 14 (Event 19) in Table 1. An inverse-*S* sigmoidal shape is shown in the white circle.

mean of 25.9 hr. Meanwhile, the average of $\langle V_{\rm MC}\rangle$ is found to be 470.5 km s^{-1}.

3. MAGNETIC CLOUD FITTING MODEL

In order to calculate magnetic fluxes and helicities carried by a MC from the Sun, we model the MC using the constant-α force-free field solution of the equation $\nabla \times \mathbf{B} = \alpha \mathbf{B}$ in cylindrical coordinates assuming cylindrical symmetry. Thus, the field is given by

$$\mathbf{B} = s B_0 J_1(\alpha r)\hat{\phi} + B_0 J_0(\alpha r)\hat{z}, \quad (1)$$

where s is the handedness or chirality of the MC, B_0 is the strength of the field at the MC axis, J_n is the Bessel function of the first kind of order n, and r is the radial distance from the cylinder axis. The magnetic flux ($F_{\rm MC}$) can be easily calculated from Equation (1)

$$F_{\rm MC} = \int \mathbf{B}\cdot\hat{z}d\mathbf{A} = \frac{2\pi J_1(x_{01})}{x_{01}} B_0 R_{\rm MC}^2, \quad (2)$$

where $dA = 2\pi r dr$, x_{01} is the first zero of $J_0(x)$ ($x_{01} = 2.4048$) with the force-free parameter (α) defined as $\alpha R_{\rm MC} = x_{01}$, and $R_{\rm MC}$ is the radius of MC. Thus, $F_{\rm MC}$ is given as

$$F_{\rm MC} = 2\pi(0.21588) B_0 R_{\rm MC}^2, \quad (3)$$

where the numerical factor is $\frac{J_1(2.4048)}{2.4048}$ (Leamon et al. 2004). Also, the relative helicity per unit length is given by

$$\frac{H_{\rm MC}}{L} = \frac{4\pi B_0^2}{\alpha}\int_0^{R_{\rm MC}} J_1^2(\alpha r) r dr \quad (4)$$

(Dasso et al. 2005). The parameters needed to calculate $F_{\rm MC}$ and $H_{\rm MC}$ are obtained from the result of the cylinder model following Marubashi & Lepping (2007). This model includes a self-similar expansion that was originally proposed by Farrugia et al. (1992), with a slight modification based on the proposal by Shimazu & Vandas (2002). The method of fitting and the relevant expressions are described in Section 3.1 and Appendix A of Marubashi & Lepping (2007). In this model the radius ($R_{\rm MC}$) varies with time, and correspondingly B_0 and α change with time as well because of the effect of self-similar expansion

$$R_{\rm MC} \propto (1 + Et), \quad (5)$$

$$\alpha \propto (1 + Et), \quad (6)$$

$$B_0 \propto (1 + Et)^{-2}, \quad (7)$$

where E is a parameter associated with the expansion rate. For the calculation of magnetic flux and helicity of MC, we use the parameters at time $t = 0$ when the spacecraft encounters the MC first (e.g., $R_{\rm MC}$ at $t = 0$). Note that $F_{\rm MC}$ is independent of the expansion (see Equation (3)), and the expansion effect on $H_{\rm MC}/L$ is expressed in α in Equation (4), due to expansion in the direction of the MC axis (Shimazu & Vandas 2002).

Table 2 gives the results obtained from the cylinder model fitting. Columns 2–8 show the fitted parameter: the latitude and longitude angles of the field vector at the cylinder axis (θ and ϕ), the intensity of the magnetic field at the cylinder axis (B_0), the impact parameter (p), the radius of the MC cylinder (R_0), the velocity of MC at the time of encounter (U_0), and the expansion rate (E), respectively. R_0 is found to be between 4.47×10^{10} cm (0.003 AU) and 3.33×10^{12} cm (0.222 AU) and its average is 1.53×10^{12} cm (0.105 AU). Next three columns show α, $F_{\rm MC}$, and magnetic helicity per unit length ($H_{\rm MC}/L$). $F_{\rm MC}$ varied from 1.25×10^{18} to 4.69×10^{21} Mx with the average of 1.10×10^{21} Mx that is similar to 1.61×10^{21} Mx calculated by Leamon et al. (2004). $|H_{\rm MC}|/L$ varied from 1.76×10^{33} to 1.10×10^{42} Mx^2 with the average of 1.20×10^{41} Mx^2. The negative sign in 9 and 11 columns indicates that the MC has left-handed chirality. Fifteen out of 34 MCs have right-handed and 19 MCs have left-handed chirality. Comparing with the shape of the AR sigmoid in Table 1, we found that all sigmoids of ARs have the same chirality as that of the corresponding MCs except for Event 4. For the correlation study, we use the absolute value of magnetic helicity. The last column gives the relative errors, $\Delta/B_{\rm max}$, where $B_{\rm max}$ is the maximum of the observed magnetic field intensity within the MC, and Δ is the rms deviation between the observed magnetic fields, $\boldsymbol{B}_{\rm obs}(t_i)$, and the model magnetic fields, $\boldsymbol{B}_{\rm mod}(t_i)1$ ($i = 1, \ldots, N$):

$$\triangle = \sqrt{\sum_i \{\boldsymbol{B}_{\rm obs}(t_i) - \boldsymbol{B}_{\rm mod}(t_i)\}^2/N}. \quad (8)$$

Figure 2 shows one example observed by *WIND* on 1997 October 10 (Event 6 in Table 1). From top to bottom, each panel gives the magnetic field intensity, the X, Y, and Z components of the magnetic field in the geocentric solar ecliptic (GSE) coordinates, the ratio of standard deviations of data to the average intensities, the solar wind speed, the proton density, the proton temperature, and the plasma β based on protons, respectively. The thick solid lines are the best-fit linear force-free cylinder model to the observed field (see Table 2). The characteristic linear decrease in the solar wind speed indicates the MC expansion. The bottom panels show the magnetic field vectors projected on the X–Y, X–Z, and Y–Z planes, respectively. The rotation of the magnetic field can be easily seen in such diagrams. Two vertical lines indicate the chosen start and end times of the MC. To determine the most likely values of these parameters, we have tried several possible ones based on the rotation pattern of magnetic field and selected the one that yields the lowest value of $\Delta/B_{\rm max}$.

4. RESULTS

In Figure 3, we compare the helicity $|H_{\rm MC}|/L$ with (a) the square of mean velocity of MC ($\langle V_{\rm MC}\rangle^2$) and (b) the square of

Table 2
Magnetic Clouds: Fit Parameters and Inferred Quantities

Event No.	θ (°)	ϕ (°)	B_0 (nT)	p	R_0 (cm)	U_0 (km s^{-1})	$E\times48$ (/48 hr)	α (cm^{-1})	F_{MC} (Mx)	H_{MC}/L (Mx^2 AU^{-1})	Δ/B_{max}
1	−16.5	235.4	19.4	0.00	1.26E + 12	438.0	0.48	2.29E − 11	4.19E + 20	5.51E + 39	0.226
2	−9.9	161.6	37.0	−0.57	4.36E + 11	464.5	1.06	−1.90E − 10	9.55E + 19	−9.95E + 37	0.258
3	−4.6	50.8	24.2	0.59	8.29E + 11	435.8	0.37	−5.24E − 11	2.25E + 20	−1.06E + 39	0.271
4	73.2	44.3	23.5	0.55	2.02E + 12	421.4	0.78	−8.86E − 12	1.30E + 21	−8.45E + 40	0.193
5	26.1	8.6	16.1	0.86	2.07E + 12	450.0	0.07	−8.42E − 12	9.36E + 20	−4.41E + 40	0.304
6	−19.4	246.9	17.8	−0.42	1.69E + 12	402.3	0.54	1.26E − 11	6.87E + 20	2.01E + 40	0.220
7	19.5	230.2	17.8	0.06	1.77E + 12	426.4	0.18	1.15E − 11	7.57E + 20	2.48E + 40	0.268
8	−15.7	166.3	41.4	0.22	3.40E + 11	511.6	3.38	3.11E − 10	6.49E + 19	3.60E + 37	0.300
9	53.4	19.8	25.7	0.02	1.59E + 12	380.3	0.79	−1.42E − 11	8.80E + 20	−3.15E + 40	0.191
10	−18.3	334.4	10.8	0.36	1.28E + 12	396.7	−0.77	2.21E − 11	2.39E + 20	1.86E + 39	0.345
11	29.2	76.6	16.0	0.49	2.11E + 12	337.2	0.34	−8.08E − 12	9.68E + 20	−4.84E + 40	0.218
12	42.8	340.8	24.0	−0.97	2.56E + 12	534.2	1.85	−5.51E − 12	2.14E + 21	−2.82E + 41	0.264
13	35.5	131.3	17.3	0.09	1.97E + 12	460.5	0.79	−9.26E − 12	9.08E + 20	−4.15E + 40	0.233
14	−2.1	359.5	46.1	0.94	4.47E + 10	406.6	0.53	−1.80E − 8	1.25E + 18	−1.76E + 33	0.154
15	−32.8	52.2	24.5	0.02	1.82E + 12	468.3	1.06	1.09E − 11	1.10E + 21	5.43E + 40	0.387
16	−53.1	174.7	27.5	0.64	1.67E + 12	381.4	0.31	1.29E − 11	1.04E + 21	4.65E + 40	0.314
17	−37.9	99.7	29.8	0.46	1.47E + 12	411.3	0.44	−1.66E − 11	8.75E + 20	−2.86E + 40	0.198
18	59.1	19.8	24.8	−0.66	1.44E + 12	377.6	0.57	1.73E − 11	6.97E + 20	1.81E + 40	0.273
19	18.9	61.5	74.9	−0.02	1.91E + 12	960.6	1.71	−9.91E − 12	3.71E + 21	−6.71E + 41	0.172
20	31.4	333.6	20.9	−0.36	7.96E + 11	461.6	0.62	−5.69E − 11	1.79E + 20	−6.38E + 38	0.310
21	10.4	136.8	44.7	−0.50	1.73E + 12	590.3	0.82	−1.21E − 11	1.81E + 21	−1.39E + 41	0.291
22	12.5	34.9	26.9	−0.01	1.03E + 12	408.7	2.44	3.37E − 11	3.86E + 20	3.99E + 39	0.387
23	−30.7	47.0	19.1	−0.71	1.92E + 12	402.0	0.11	9.81E − 12	9.55E + 20	4.48E + 40	0.242
24	−20.4	22.0	34.0	0.96	1.13E + 12	389.3	1.02	−2.81E − 11	5.88E + 20	−1.00E + 40	0.155
25	11.2	119.1	26.2	−0.21	1.66E + 12	528.7	0.13	−1.30E − 11	9.78E + 20	−4.08E + 40	0.184
26	−65.5	128.8	25.3	0.10	2.89E + 12	371.9	1.49	−4.33E − 12	2.87E + 21	−6.15E + 41	0.305
27	−46.9	312.5	19.3	0.46	1.34E + 12	359.9	0.59	−2.01E − 11	4.69E + 20	−7.25E + 39	0.170
28	10.1	210.8	18.0	0.70	9.61E + 11	627.8	0.94	3.90E − 11	2.25E + 20	1.24E + 39	0.336
29	49.2	32.4	19.3	−0.13	1.77E + 12	379.4	0.46	1.15E − 11	8.22E + 20	2.92E + 40	0.278
30	34.4	284.5	16.4	0.12	3.33E + 12	434.8	−0.02	3.25E − 12	2.46E + 21	4.84E + 41	0.226
31	−16.3	322.3	23.8	−0.71	1.90E + 12	472.7	1.05	9.96E − 12	1.17E + 21	6.70E + 40	0.163
32	−64.9	158.3	75.0	0.29	1.04E + 12	592.2	1.61	3.33E − 11	1.10E + 21	3.22E + 40	0.187
33	−22.0	267.5	39.9	0.13	1.63E + 12	766.3	0.49	−1.35E − 11	1.44E + 21	−8.69E + 40	0.348
34	47.6	176.9	85.6	0.53	2.01E + 12	827.3	3.42	−8.95E − 12	4.69E + 21	−1.10E + 42	0.186
Average			29.8		1.58E + 12	478.8			1.10E + 21	1.20E + 41[a]	

Note.
[a] Averaged magnetic helicity is calculated by absolute value ($|H_{MC}|/L$).

CME initial speed (V^2_{CME}). In this plot, we add a line fit, the linear correlation coefficient (R), the standard deviation (SD), the number of samples (N), and the probability (P). The open and closed circles indicate the right-handed and left-handed chiralities, respectively. We see from the figure that $|H_{MC}|/L$ and V^2_{CME} have positive correlation ($R = 0.39$) while there is no significant correlation ($R = 0.21$) between $|H_{MC}|/L$ and $\langle V_{MC}\rangle^2$.

Figure 4 shows two scatter plots of (a) F_{MC} and $\langle V_{MC}\rangle^2$, and (b) F_{MC} and V^2_{CME}. The correlation coefficients are 0.25 for the relationship between F_{MC} and $\langle V_{MC}\rangle^2$ and 0.43 for the relationship between F_{MC} and V^2_{CME}. The scatter patterns are almost the same as Figure 3.

Now we consider two criteria to select the events that provide more reliable fitting results. One is the impact parameter (p), the distance from the MC axis to the spacecraft trajectory normalized by MC radius, R_{MC}. Since the model fitting is to reproduce the observed magnetic field data inside the MC, the fitting result can be more reliable when the spacecraft passes through as close as possible to the MC axis. Riley et al. (2004) showed that accuracy of fitting result decreases markedly with increasingly glancing encounters from the blind test for five different flux rope fitting techniques. For this reason, we ignored the events whose impact parameters are greater than 0.5. The other criterion is concerned with several long-duration MC events. In some cases, the straight cylindrical model is not sufficient to fit a given MC if it has a large curvature or the spacecraft encounters the flank side of the MC. Marubashi & Lepping (2007) presented MC events the structure of which can be understood only by a torus model, and that correspond to the case when the spacecraft traversed the flank of the MC loop (Group A in their paper). Since four events (Events 5, 12, 15, and 26) belong to this Group A, we have removed them to avoid inappropriate interpretation limited by the cylinder model.

Using 19 events only left after removing the less appropriate events, we found that the correlation coefficient between $|H_{MC}|/L$ and V^2_{CME} increases from 0.39 to 0.56, and the one between F_{MC} and V^2_{CME} from 0.43 to 0.64, as shown in Figure 5. The high values of the correlations between $|H_{MC}|/L$ and V^2_{CME} (and/or between F_{MC} and V^2_{CME}) indicate that a CME with larger magnetic flux and/or helicity is launched from the Sun with a higher initial speed. Although the corresponding diagrams are not shown here, R of $\langle V_{MC}\rangle^2$ is still less than that of V^2_{CME} (see Table 3). Gopalswamy et al. (2000) found that slow CMEs are accelerated and fast CMEs are decelerated while

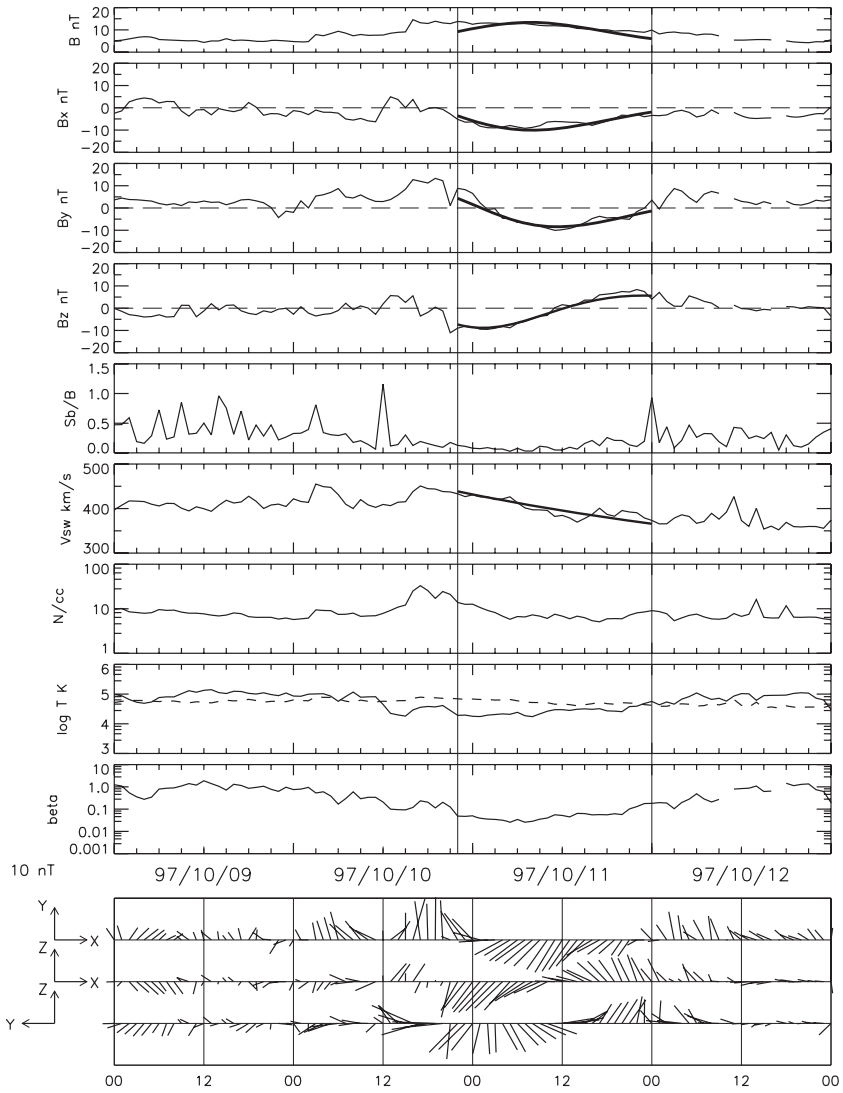

Figure 2. Magnetic cloud event on 1997 January 10–11 (Event 6 in Table 1). Fitting results are shown in thick solid lines. Two vertical lines give the MC boundaries.

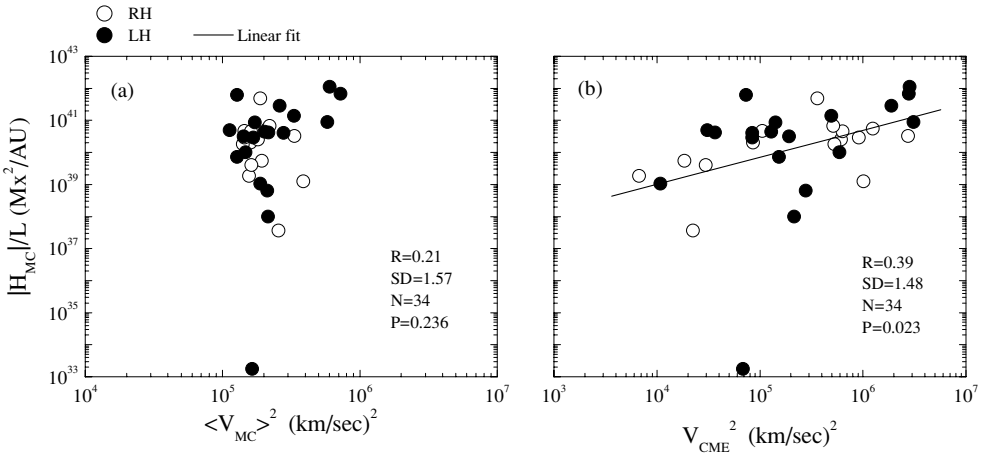

Figure 3. Scatter diagrams of (a) $|H_{\rm MC}|/L$ vs. $\langle V_{\rm MC}\rangle^2$ and (b) $|H_{\rm MC}|/L$ vs. $V_{\rm CME}^2$ for 34 CME–MC pairs. The open (solid) circles represent right-handed (left-handed) MCs. The straight lines are obtained by the linear fitting. The linear correlation coefficient R, standard deviation SD, number of data points N, and the probability P are shown in both (a) and (b).

propagating through the interplanetary space. Since the speeds of CMEs near the Earth are influenced, we can expect the lower correlation coefficient with $\langle V_{\rm MC}\rangle^2$.

We also have investigated the correlations of MC flux (MC helicity) with the mean velocity of the MC, the CME initial speed, and the CME kinetic energy for all events (34), the events

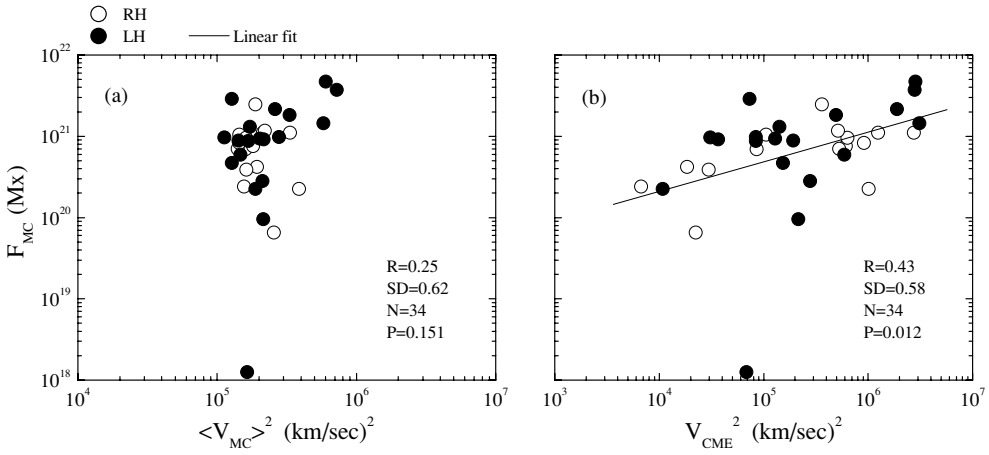

Figure 4. Same as Figure 3(a) for F_{MC} vs. $\langle V_{MC}\rangle^2$ and (b) F_{MC} vs. V^2_{CME}.

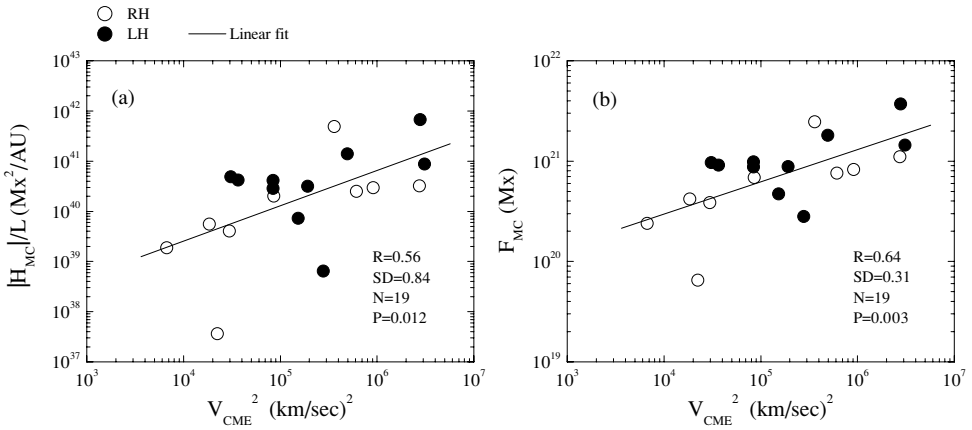

Figure 5. Scatter diagrams of (a) $|H_{MC}|/L$ vs. $\langle V_{MC}\rangle^2$ and (b) F_{MC} vs. V^2_{CME} for selected 19 events.

Table 3
Correlation Coefficients for Each Case

Parameter	Events	Nos. of data[a]	$\langle V_{MC}\rangle$	$\langle V_{MC}\rangle^2$	V_{CME}	V^2_{CME}	E_{CME}
	All	(34, 25)	0.28	0.25	0.43	0.43	0.43
MC	nLM[b]	(30, 22)	0.32	0.30	0.46	0.46	0.51
flux	p (<0.5)	(21, 16)	0.34	0.29	0.50	0.57	0.54
	nLM+p	(19, 15)	0.44	0.40	0.57	0.64	0.65
	All	(34, 25)	0.24	0.21	0.39	0.39	0.39
MC	nLM	(30, 22)	0.28	0.25	0.42	0.42	0.47
helicity	p (<0.5)	(21, 16)	0.26	0.21	0.42	0.50	0.46
	nLM+p	(19, 15)	0.36	0.31	0.50	0.56	0.57

Notes.

[a] Two different numbers presented in the parenthesis indicate CME–MC pairs used in each correlation study. First is the number of pairs for comparing MC flux (MC helicity) with $\langle V_{MC}\rangle$, $\langle V_{MC}\rangle^2$, V_{CME} and V^2_{CME}. The second is for E_{CME}. Note that several events have no CME kinetic energy information in the CME catalog.

[b] Excludes long-duration MCs (Group A in Marubashi & Lepping (2007)).

excluding long duration (30), the events with small impact parameter (21), and those with the small impact parameter without long-duration MC (19), respectively. The results of all these comparisons are summarized in Table 3. We found that the correlation coefficients increase for every case when we apply the above criteria for event selection. Our correlation study reveals that the correlation between F_{MC} and V_{CME} or E_{CME} is stronger than between $|H_{MC}|/L$ and V_{CME} or E_{CME}. The biggest correlation coefficient ($R = 0.65$) is found for the relationship between F_{MC} and E_{CME}.

5. CONCLUSIONS AND DISCUSSION

In this study, we have compared two parameters (F_{MC} and $|H_{MC}|/L$) of MCs with the initial speed and kinetic energy of CMEs, and the mean velocity of MC. We have calculated the correlation coefficients using 34 CME–MC pairs. As a result, we have obtained the following results:

1. We found that F_{MC} and $|H_{MC}|/L$ are positively correlated with V^2_{CME}. This result is consistent with the conclusion of Su et al. (2007) and implies that magnetic flux and/or helicity released in ARs play an important role in the eruption of CMEs.
2. The correlation coefficient increased when less appropriate events are removed by two criteria. One is the impact parameter. When we consider the MCs with small impact parameter ($p < 0.5$), the correlation coefficients increased (see Table 3). This result implies that the parameters obtained for MCs with small p are more reliable when applying the fitting result to studies of MC internal structure. Second, by ignoring the long-duration MCs whose flank side is observed, we also found that the correlation coefficients increased.
3. The correlation of the parameters of MC with ($\langle V_{MC}\rangle^2$) is significantly low. The previous study by Lynch et al.

(2005) concluded that the fastest MCs carry the most flux and helicity, but no significant correlation exists between the helicity and the average radial speed in MCs. This lack of correlation for $\langle V_{\rm MC}\rangle^2$ is due to the fact that a MC is already accelerated (or decelerated) before it reaches the 1 AU distance from the Sun while magnetic flux and magnetic helicity are conserved. Thus, the initial speed of a CME is preferred to the speed of a MC when the relationships among CME–MC parameters are investigated.

4. There are a couple of concerns to be considered in the investigation of the observed correlation between $|H_{\rm MC}|/L$ and $V^2_{\rm CME}$. One is whether the identification of CME–MC pairs is reliable or not. We found that the shapes of 25 AR sigmoids imply the same handedness of ARs as the magnetic helicity of the associated MCs. This supports that our identification of CME–MC pairs is reasonable. The other concern arises from the fact that the helicity was inferred from the measurements by one probe and the distribution of magnetic helicity along the MC axis is unknown. Practically, it is hard to investigate whether the field twist along the MC axis is uniform or not using only one satellite observation. Even with two or more satellites, if they are too close to each other, a similar problem still occurs. Consequently, the need arises of simultaneous multi-satellite observations that are separated enough from each other. This work can be performed by missions like *Solar TErrestrial RElations Observatory* (*STEREO*).

In summary, by examining 34 pairs of CMEs and MCs, we found that (1) $V^2_{\rm CME}$ has a good correlation with $F_{\rm MC}$ and $|H_{\rm MC}|/L$ (substitute of magnetic flux and magnetic helicity in ARs) and (2) $\langle V_{\rm MC}\rangle^2$ is not correlated with $F_{\rm MC}$ and $|H_{\rm MC}|/L$. Our results support the idea that the speed of a CME is related to the magnetic helicity of the source solar AR, and probably to its free energy, supposing the helicity is closely related to the free magnetic energy of the source region.

We really appreciate the referee's constructive comments. We are indebted to the *WIND* SWE, and MFI teams for the *WIND* data, to the *ACE* MAG and SWEPAM instrument teams and the *ACE* Science Center for the *ACE* data, and to the *Yohkoh* SXT team and *GOES* SXI team for solar X-ray images. This work was supported by the "Development of Korean Space Weather Center," the project of KASI, the KASI basic research fund, and the Korea Research Foundation Grant (KRF-2005-070-C00059). This work has been supported by the WCU Grant (No. R31-10016) funded by the Korean Ministry of Education, Science and Technology.

REFERENCES

Berger, M. A. 1984, Geophys. Astrophys. Fluid Dyn., 30, 79
Cane, H. V., & Richardson, I. G. 2003, J. Geophys. Res., 108, 1156
Chen, A. Q., Chen, P. F., & Fang, C. 2006, A&A, 456, 1153
Chen, J. 1989, ApJ, 338, 453
Chen, J. 1996, J. Geophys. Res., 101, 27499
Dasso, S., et al. 2005, Adv. Space Res., 35, 711
Farrugia, C. J., Burlaga, L. F., Osherovich, V. A., & Lepping, R. P. 1992, in Proc. 3rd COSPAR Colloquium, Solar Wind Seven, ed. E. Marsch & R. Schwenn (Oxford: Pergamon), 611
Forbes, T. G. 2000, J. Geophys. Res., 105, 23153
Forbes, T. G., & Priest, E. R. 1995, ApJ, 446, 377
Gopalswamy, N., et al. 2000, Geophys. Res. Lett., 27, 145
Kang, S.-M., et al. 2006, J. Geophys. Res., 111, A05102
Kim, K.-H., Moon, Y.-J., & Cho, K.-S. 2007, J. Geophys. Res., 112, A05104, doi:10.1029/2006JA011904
Leamon, R. J., et al. 2004, J. Geophys. Res., 109, A05106
Lepping, R. P., et al. 1995, Space Sci. Rev., 71, 207
Lin, J., Raymond, J. C., & van Ballegooijen, A. A. 2004, ApJ, 602, 422
Lindsay, G. M., Luhmann, J. G., Russell, C. T., & Gosling, J. T. 1999, J. Geophys. Res., 104, 12515
Liu, Yang 2007, Adv. Space Res., 39, 1767
Luoni, M. L., Mandrini, C. H., Dasso, S., van Driel-Gesztelyi, L., & Demoulin, P. 2005, J. Atmos. Sol.-Terr. Phys., 67, 1734
Lynch, B. J., Antiochos, S. K., MacNeice, P. J., Zurbuchen, T. H., & Fisk, L. A. 2004, ApJ, 617, 589
Lynch, B. J., Gruesbeck, J. R., Zurbuchen, T. H., & Antiochos, S. K. 2005, J. Geophys. Res., 110, A08107
Mandrini, C. H., Pohjolainen, S., Dasso, S., Green, L. M., Demoulin, P., van Driel-Gesztelyi, L., Copperwheat, C., & Foley, C. 2005, A&A, 434, 725
Manoharan, P. K., Gopalswamy, N., Yashiro, S., Lara, A., Michalek, G., & Howard, R. A. 2004, J. Geophys. Res., 109, A06109
Marubashi, K., & Lepping, R. P. 2007, Ann. Geophys., 25, 2453
McComas, D. J., Bame, S. J., Barker, P., Feldman, W. C., Philips, J. L., Riley, P., & Griffee, J. W. 1998, Space Sci. Rev., 86, 563
Ogilvie, K. W., et al. 1995, Space Sci. Rev., 71, 55
Pevtsov, A. A., & Canfield, R. C. 2001, J. Geophys. Res., 106, 25,191
Phillips, A. D., MacNeice, P. J., & Antiochos, S. K. 2005, ApJ, 624, L129
Qiu, J., et al. 2007, ApJ, 659, 758
Riley, P., et al. 2004, J. Atmos. Sol.-Terr. Phys., 67, 1734
Shimazu, H., & Vandas, M. 2002, Earth Planets Space, 54, 783
Smith, C. W., L'Heureux, W. J., Ness, N. F., Acuna, M. H., Burlaga, L. F., & Scheifele, J. 1998, Space Sci. Rev., 86, 613
Su, Y., et al. 2007, ApJ, 665, 1448
Titov, V. S., & Dèmoulin, P. 1999, A&A, 351, 707
Venkatakrishnan, P., & Ravindra, B. 2003, Geophys. Res. Lett., 30, 2181
Yurchyshyn, V., Wang, H., & Abramenko, V. 2004, Space Weather, 2, S02001
Zhang, J., et al. 2007, J. Geophys. Res., 112, A10102